

Co^{II}₄, Co^{II}₇, and a Series of Co^{II}₂Ln^{III} (Ln^{III} = Nd^{III}, Sm^{III}, Gd^{III}, Tb^{III}, Dy^{III}) Coordination Clusters: Search for Single Molecule Magnets

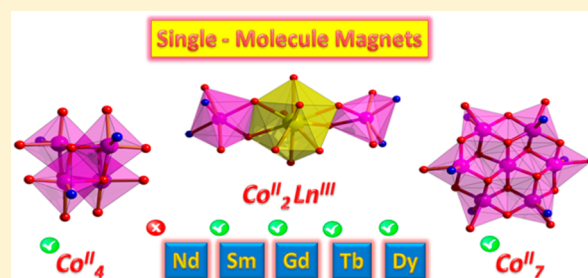
Ritwik Modak,[§] Yeasin Sikdar,[§] Annaliese E. Thuijs,[†] George Christou,^{*,†} and Sanchita Goswami^{*,§}

[§]Department of Chemistry, University of Calcutta, 92, A. P. C. Road, Kolkata 700009, India

[†]Department of Chemistry, University of Florida, Gainesville, Florida 32611-7200, United States

Supporting Information

ABSTRACT: We report herein the syntheses and investigation of the magnetic properties of a Co^{II}₄ compound, a series of trinuclear Co^{II}₂Ln^{III} (Ln^{III} = Nd^{III}, Sm^{III}, Gd^{III}, Tb^{III}, Dy^{III}) complexes, and a Co^{II}₇ complex. The homometallic Co^{II}₄ core was obtained from the reaction of Ln(NO₃)₃·xH₂O/Co(NO₃)₂·6H₂O/H₂vab/Et₃N in a 0.5:0.5:1:2 ratio in methanol. Variation in synthetic conditions was necessary to get the desired Co^{II}–Ln^{III} complexes. The Co^{II}–Ln^{III} assembly was synthesized from Ln(NO₃)₃·xH₂O/Co(OAc)₂·4H₂O/H₂vab/NaOMe in a 0.4:0.5:1:1 ratio in methanol. The isostructural Co^{II}₂Ln^{III} complexes have a core structure with the general formula [Co₂Ln(Hvab)₄(NO₃)](NO₃)₂·MeOH·H₂O, (where H₂vab = 2-[(2-hydroxymethyl-phenylimino)-methyl]-6-methoxy-phenol) with simultaneous crystallization of Co^{II}₇ complex in each reaction. The magnetic investigation of these complexes reveals that both homometallic complexes and four Co^{II}–Ln^{III} complexes (except Co^{II}–Nd^{III}) display behavior characteristic of single molecule magnets.



1. INTRODUCTION

Since the first single molecule magnet (SMM), Mn₁₂Ac, was discovered in the 1990s, many magnetic molecules exhibiting slow relaxation of magnetization have been synthesized and magnetically characterized. A large negative zero-field splitting parameter (*D*) and large ground state spin (*S*) are regarded as two essential factors necessary to obtain an SMM with a high relaxation barrier (*U*_{eff}) and blocking temperature (*T*_B). These factors play a crucial role in the potential technological applications of SMMs, such as quantum computers, spintronic devices, and high-density information storage.¹

In order to increase spin, magnetic anisotropy, and subsequently the energy barrier, much of the current SMM research has been shifted toward 3d–4f aggregates due to the strong magnetic anisotropy of 4f ions, which can provide an essential basis for tuning the properties of technologically applicable magnetic materials.²

As Co^{II} possesses significant magnetic anisotropy, the combination of Co^{II} with Ln^{III} ions might present a potentially interesting protocol to design SMMs. Recent literature reports of Co^{II}–Ln^{III} compounds stimulated us to investigate more Co^{II}–Ln^{III} entities to further explore the effect of magnetic interactions between Co^{II} and Ln^{III} on SMM behavior.³ The difficulty encountered when developing new strategies for the generation of Co^{II}–Ln^{III} compounds with promising magnetic output is to determine the contribution of the lanthanide ion to the magnetic properties by comparing a series of Co^{II}–Ln^{III} aggregates. Keeping these in mind, we have employed a vanillin-based versatile Schiff base ligand, H₂vab, for the generation of Co^{II}–Ln^{III} complexes. In this paper, synthetic

experience and adaptability are demonstrated while aiming to synthesize new Co^{II}–Ln^{III} compounds. One synthetic scheme using Co(NO₃)₂·6H₂O, Ln(NO₃)₃·xH₂O, H₂vab, and Et₃N yielded only a new Co^{II}₄ cubane compound, whereas a modified synthetic approach involving Ln(NO₃)₃·xH₂O, Co(OAc)₂·4H₂O, H₂vab, and NaOMe produced desirable Co^{II}₂Ln^{III} compounds along with the simultaneous generation of a Co^{II}₇ compound.

Herein, we report the synthesis and characterization of [Co^{II}₄(vab)₄(H₂O)₄]·4THF·4H₂O (**1**), an isostructural series of trinuclear Co^{II}₂Ln^{III} compounds with the general formula, [Co₂Ln(Hvab)₄(NO₃)](NO₃)₂·MeOH·H₂O, (where H₂vab = 2-[(2-hydroxymethyl-phenylimino)-methyl]-6-methoxy-phenol and Ln^{III} = Nd^{III} **2**, Sm^{III} **3**, Gd^{III} **4**, Tb^{III} **5**, Dy^{III} **6**) and [Co^{II}₇(vab)₆](NO₃)₂·2H₂O (**7**). To date, only a few Co^{II}₂Ln^{III} cores are reported in the literature.^{3a–c,4} The rarity of this series of heterometallic Co^{II}–Ln^{III} complexes led us to study the magnetic properties of such systems and evaluate their potential as SMMs.

2. EXPERIMENTAL SECTION

2.1. General Information. 2-Amino benzyl alcohol, *o*-vaniline, Ln(NO₃)₃·xH₂O, and sodium methoxide were procured from Aldrich Chemical Co. Inc. (Germany) and used as received. Co(NO₃)₂·6H₂O, Co(OAc)₂·4H₂O, and triethylamine were purchased from SRL Pvt. Ltd., Mumbai, India. Commercially available solvents were purified according to standard literature methods.^{5a} All the reactions were

Received: June 9, 2016

Published: October 3, 2016

carried out under aerobic conditions. The Schiff base ligand 2-[(2-hydroxymethyl-phenylimino)-methyl]-6-methoxy phenol (H_2vab) was prepared according to literature procedures.^{5b} Elemental (C, H, and N) analyses were conducted by a Perkin–Elmer 2400 II analyzer. Fourier transform infrared (FTIR) spectra were recorded in the region from 400–4000 cm^{-1} on a Perkin–Elmer RXI FTIR spectrophotometer with samples prepared as KBr disks. ESI–MS experiments were carried out in Waters on a MICROMASS Q-TOF mass spectrometer in LC–MS grade solvent. An energy dispersive X-ray (EDX) analysis was done by field emission scanning electron microscopy (FESEM–JEOL JSM 7600F). Powder X-ray diffraction (PXRD) patterns were acquired for complexes **2** and **6** using a PANalytical XPERT-PRO diffractometer (Netherlands). Magnetic measurements were performed at the Department of Chemistry, University of Florida. Variable temperature *dc* and *ac* magnetic susceptibility data were collected on dried solids using a Quantum Design MPMS-XL SQUID susceptometer equipped with a 7 T magnets and operating in the 1.8–300 K range. Samples were embedded in solid eicosane to prevent torquing. Pascal's constants were used to estimate the diamagnetic correction, which was subtracted from the experimental susceptibility to give the molar paramagnetic susceptibility (χ_M).

2.2. Synthesis of $[Co_4(vab)_4(H_2O)_4] \cdot 4THF \cdot 4H_2O$ (1). $Co(NO_3)_2 \cdot 6H_2O$ (0.145 g, 0.5 mmol) and $Ln(NO_3)_3 \cdot xH_2O$ (0.5 mmol) were dissolved in 10 mL of methanol followed by the dropwise addition of 15 mL of methanolic solution of H_2vab (0.257 g, 1 mmol) under stirring conditions. To the resulting solution, Et_3N (0.277 mL, 2 mmol) was added dropwise. The resulting mixture was stirred for 2 h, and consequently a precipitate was formed. After complete evaporation of the solvent, the reddish precipitate was dissolved in a minimum amount of THF. X-ray diffraction quality single crystals were obtained after 2 days in 0.079 g, 46% (based on Co) yield. FT-IR (KBr), cm^{-1} : 3431(*br*), 1608(*vs*), 1542(*m*), 1463(*s*), 1442(*m*), 1230(*s*), 1185(*m*), 758(*w*), 737(*m*), 560(*w*), 538(*w*), 446(*w*). C/H/N analysis, calcd. for $C_{76}H_{100}N_4O_{24}Co_4$ (1689.32 $g\ mol^{-1}$): C, 54.03; H, 5.97; N, 3.32%. Found: C, 53.85; H, 5.69; N, 3.20%.

2.3. General Procedure for the Syntheses of $[Co_2Ln(Hvab)_4(NO_3)](NO_3)_2 \cdot MeOH \cdot H_2O$ (2–6) and $[Co_7(vab)_d](NO_3)_2 \cdot 2H_2O$ (7). The trinuclear heterometallic and heptanuclear homometallic complexes were obtained by the following general synthetic methodology under aerobic conditions. A methanolic solution of NaOMe (1 equiv) was added to the methanolic solution of H_2vab (1 equiv) and was stirred for 15 min. The methanolic solution of $Ln(NO_3)_3 \cdot xH_2O$ (~0.4 equiv) was added dropwise to the ligand solution under continuous stirring. After stirring for ~4 h, solid $Co(OAc)_2 \cdot 4H_2O$ (0.5 equiv) was added, and the solution was vigorously stirred for a further ~12 h. The final reaction mixture was filtered off, and the filtrate was evaporated to dryness under reduced pressure. The red colored solid was left overnight in a vacuumed calcium chloride desiccator. The resulting solid was redissolved in a mixture of methanol/acetonitrile (1:1). Crystals of the hetero- and homometallic clusters suitable for single crystal X-ray diffraction studies were simultaneously obtained by slow diffusion of diethyl ether into this 1:1 (MeOH/MeCN) solution mixture over a period of 1 week. Two types of crystals were separated manually and washed with *n*-hexane. The specific quantities and stoichiometry of the reactants involved in each reaction, yield of the products, and their characterization data are given below.

$[Co_2Nd(Hvab)_4(NO_3)](NO_3)_2 \cdot MeOH \cdot H_2O$ (2). Quantities: H_2vab (0.257 g, 1 mmol), $Nd(NO_3)_3 \cdot 6H_2O$ (0.167 g, 0.381 mmol), $Co(OAc)_2 \cdot 4H_2O$ (0.124 g, 0.5 mmol), NaOMe (0.54 mg, 1 mmol). Yield: 0.081 g, 38% (based on Co). FT-IR (KBr), cm^{-1} : 3393(*br*), 1612(*vs*), 1553(*m*), 1467(*vs*), 1385(*vs*), 1296(*m*), 1238(*s*), 1183(*m*), 1098(*m*), 761(*m*), 740(*s*), 558(*w*), 540(*w*), 451(*w*). C/H/N analysis, calcd. for $C_{61}H_{62}N_7O_{23}Co_2Nd$ (1523.28 $g\ mol^{-1}$): C, 48.10; H, 4.10; N, 6.44%. Found: C, 47.8; H, 3.90; N, 6.04%.

$[Co_2Sm(Hvab)_4(NO_3)](NO_3)_2 \cdot 1MeOH \cdot H_2O$ (3). Quantities: H_2vab (0.257 g, 1 mmol), $Sm(NO_3)_3 \cdot 6H_2O$ (0.169 g, 0.381 mmol), $Co(OAc)_2 \cdot 4H_2O$ (0.124 g, 0.5 mmol), NaOMe (0.54 mg, 1 mmol). Yield: 0.079 g, 39% (based on Co). FT-IR (KBr), cm^{-1} : 3393(*br*),

1612(*vs*), 1553(*m*), 1467(*vs*), 1385(*vs*), 1296(*m*), 1238(*s*), 1183(*m*), 1098(*m*), 761(*m*), 740(*s*), 558(*w*), 540(*w*), 450(*w*). C/H/N analysis, calcd. for $C_{61}H_{62}N_7O_{23}Co_2Sm$ (1529.40 $g\ mol^{-1}$): C, 47.90; H, 4.09; N, 6.41%. Found: C, 47.73; H, 3.72; N, 5.98%.

$[Co_2Gd(Hvab)_4(NO_3)](NO_3)_2 \cdot 1MeOH \cdot H_2O$ (4). Quantities: H_2vab (0.257 g, 1 mmol), $Gd(NO_3)_3 \cdot 6H_2O$ (0.172 g, 0.381 mmol), $Co(OAc)_2 \cdot 4H_2O$ (0.124 g, 0.5 mmol), NaOMe (0.54 mg, 1 mmol). Yield: 0.073 g, 42% (based on Co). FT-IR (KBr), cm^{-1} : 3394(*br*), 1612(*vs*), 1554(*m*), 1465(*vs*), 1385(*vs*), 1296(*m*), 1238(*s*), 1183(*m*), 1098(*m*), 761(*m*), 740(*s*), 556(*w*), 540(*w*), 452(*w*). C/H/N analysis, calcd. for $C_{61}H_{62}N_7O_{23}Co_2Gd$ (1536.29 $g\ mol^{-1}$): C, 47.69; H, 4.07; N, 6.38%. Found: C, 47.46; H, 3.77; N, 5.95%.

$[Co_2Tb(Hvab)_4(NO_3)](NO_3)_2 \cdot MeOH \cdot H_2O$ (5). Quantities: H_2vab (0.257 g, 1 mmol), $Tb(NO_3)_3 \cdot 5H_2O$ (0.165 g, 0.381 mmol), $Co(OAc)_2 \cdot 4H_2O$ (0.124 g, 0.5 mmol), NaOMe (0.54 mg, 1 mmol). Yield: 0.081 g, 38% (based on Co). FT-IR (KBr), cm^{-1} : 3395(*br*), 1611(*vs*), 1553(*m*), 1463(*vs*), 1384(*vs*), 1296(*m*), 1238(*s*), 1183(*m*), 1098(*m*), 761(*m*), 740(*s*), 556(*w*), 540(*w*), 450(*w*). C/H/N analysis, calcd. for $C_{61}H_{62}N_7O_{23}Co_2Tb$ (1537.97 $g\ mol^{-1}$): C, 47.64; H, 4.06; N, 6.38%. Found: C, 47.18; H, 3.86; N, 6.18%.

$[Co_2Dy(Hvab)_4(NO_3)](NO_3)_2 \cdot 1MeOH \cdot H_2O$ (6). Quantities: H_2vab (0.257 g, 1 mmol), $Dy(NO_3)_3 \cdot 5H_2O$ (0.167 g, 0.381 mmol), $Co(OAc)_2 \cdot 4H_2O$ (0.124 g, 0.5 mmol), NaOMe (0.54 mg, 1 mmol). Yield: 0.088 g, 35% (based on Co). FT-IR (KBr), cm^{-1} : 3395(*br*), 1611(*vs*), 1552(*m*), 1465(*vs*), 1384(*vs*), 1296(*m*), 1238(*s*), 1183(*m*), 1098(*m*), 761(*m*), 740(*s*), 555(*w*), 540(*w*), 450(*w*). C/H/N analysis, calcd. for $C_{61}H_{62}N_7O_{23}Co_2Dy$ (1541.54 $g\ mol^{-1}$): C, 47.53; H, 4.05; N, 6.36%. Found: C, 47.17; H, 3.76; N, 6.08%.

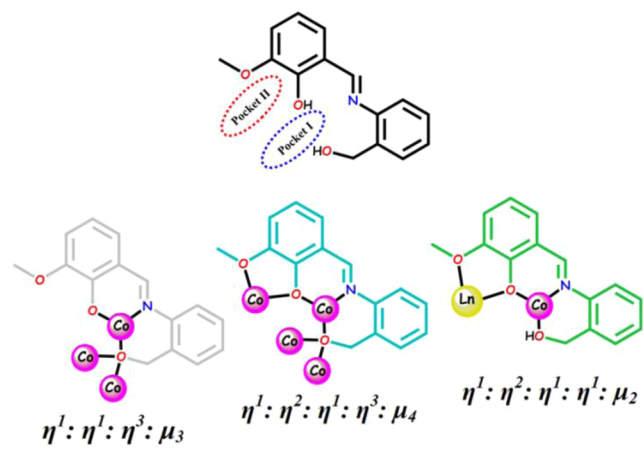
$[Co_7(vab)_d](NO_3)_2 \cdot 2H_2O$ (7). Quantities: H_2vab (0.257 g, 1 mmol), $Ln(NO_3)_3 \cdot xH_2O$ (0.381 mmol), $Co(OAc)_2 \cdot 4H_2O$ (0.124 g, 0.5 mmol), NaOMe (0.54 mg, 1 mmol). Yield: 0.065 g, 27% (based on Co). FT-IR (KBr), cm^{-1} : 3439(*br*), 1614(*vs*), 1557(*m*), 1469(*vs*), 1384(*vs*), 1300(*m*), 1242(*s*), 1181(*m*), 1095(*m*), 767(*m*), 733(*s*), 561(*w*), 541(*w*), 450(*w*). C/H/N analysis, calcd. for $C_{90}H_{82}Co_7N_8O_{26}$ (2104.15 $g\ mol^{-1}$): C, 51.37; H, 3.93; N, 5.33%. Found: C, 50.92; H, 3.66; N, 5.08%.

2.4. X-ray Structural Studies. Diffraction data for 1–7 were collected at 296 K using a Bruker Nonius Apex II CCD diffractometer with graphite monochromator and Mo K_α radiation ($\lambda = 0.71073\ \text{\AA}$). The program SMART^{6a} was used for collecting frames of data, indexing reflections, and determining lattice parameters, SAINT^{6a} was used for integration of the intensity of reflections and scaling, SADABS^{6b} for absorption correction, and SHELXTL^{6c,d} for space group, structure determination and least-squares refinements on F^2 . The structures were solved by direct methods and refined by full-matrix least-squares calculations using SHELXTL software.^{6e} All non-hydrogen atoms were refined in the anisotropic approximation against F^2 of all reflections. The location of the Ln and Co atoms were easily determined, and O, N, and C atoms were subsequently determined from a difference Fourier maps. The hydrogen atoms attached to carbon atoms were placed in calculated positions and refined riding on their parent atoms. All the hydrogen atoms of the O_{benzyl} groups, coordinated and non-coordinated water (OH_2) molecules were determined from a difference Fourier map and refined isotropically. The crystallographic figures were generated using Diamond 3.0 software.⁷ The crystal parameters of the clusters are shown in Table S1 (Supporting Information). CCDC: 1483752–1483758 contain supplementary crystallographic data for this paper. These data can be obtained free of charge from the Cambridge Crystallographic Data Centre via www.ccdc.cam.ac.uk/data_request/cif.

3. RESULTS AND DISCUSSION

3.1. Synthetic Outcome and Characterization. The ligand 2-[(2-hydroxymethyl-phenylimino)-methyl]-6-methoxyphenol (H_2vab) contains a $\{NO_3\}$ donor set that possesses both chelating and bridging capabilities with two distinct coordination pockets (I and II) as shown in Scheme 1. It is based on a basic phenol framework and contains two unsymmetrically disposed substituents. Adjacent to the phenol

Scheme 1. (Top) Structure of the Ligand H_2vab Consisting of Two Distinct Coordination Pockets and (Below) Binding Mode of the Deprotonated H_2vab



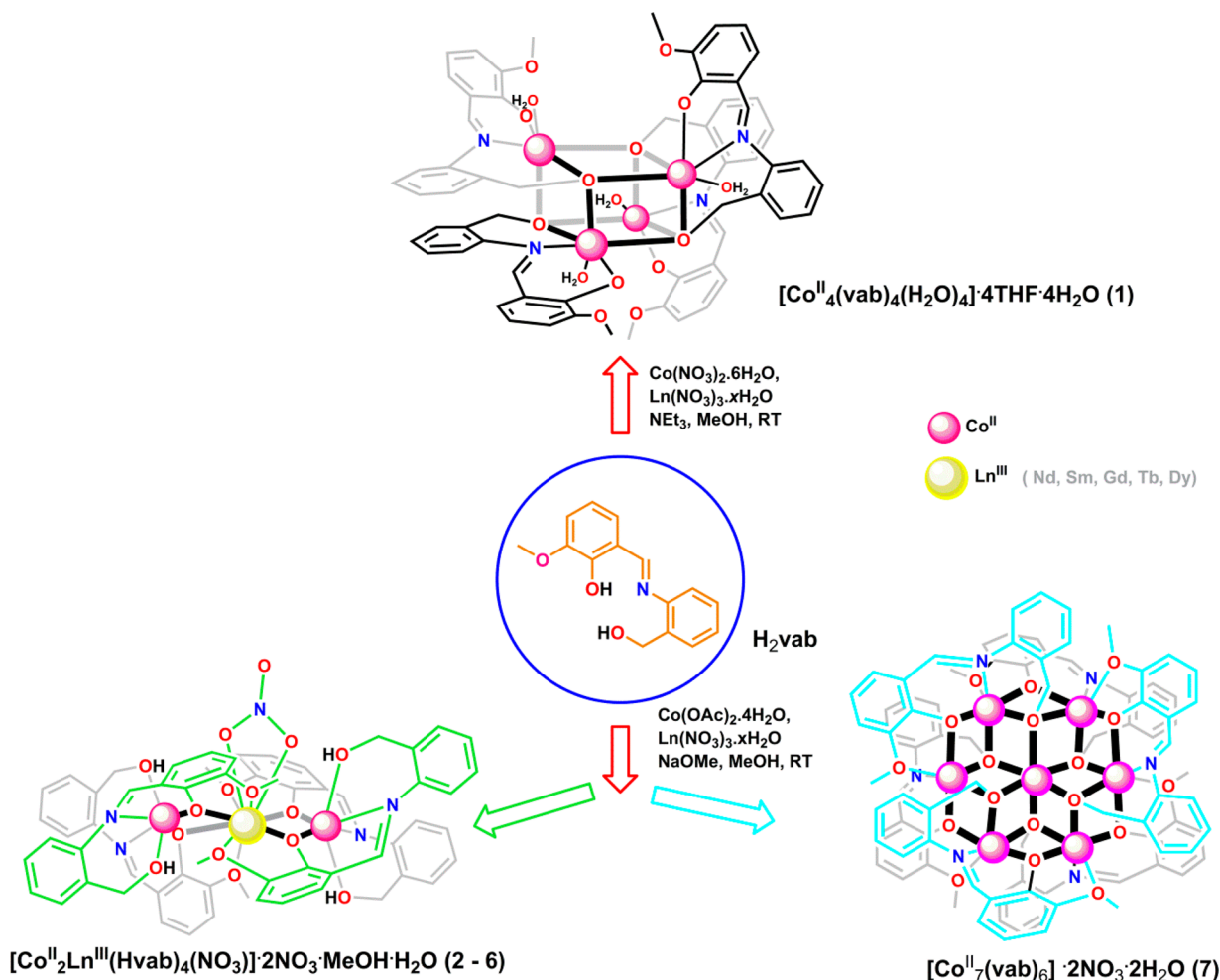
unit on one side is a 2-amino benzyl alcoholic group and on the other side a methoxy group. Previously, the four potential coordination sites (one phenoxo, one imino, one methoxo, and one benzylic alkoxo) and their multiple coordination abilities have facilitated the synthesis of several homo- and heterometallic Cu^{II}_4 ,^{5b} Ni^{II}_4 ,^{8a} $Ni^{II}Pr^{III}_{8b}$, $Ni^{II}Gd^{III}_{8b,c}$, $Ni^{II}_2La^{III}_{8b}$,

$Zn^{II}_2Pr^{III}_{8b}$, $Zn^{II}_2Gd^{III}_{8b}$, $Ni^{II}_2Tb^{III}_{2,8c}$, $Ni^{II}_2Ho^{III}_{2,8c}$ and $Ni^{II}_2Lu^{III}_{2,8c}$ cluster compounds including $Ni^{II}_2Dy^{III}_{2,8c}$ SMM. These types of Schiff bases with a vanillin backbone are well-known for their versatility as evidenced from a very recent review.⁹

As depicted in Scheme 2, the first synthetic protocol involving $Co(NO_3)_2/Ln(NO_3)_3/H_2vab/Et_3N$ in 0.5:0.5:1:2 ratio resulted a new homometallic Co^{II}_4 cubane species (complex 1). We have changed the reactant ratio and sequence of addition, but even after several attempts $Co^{II}-Ln^{III}$ aggregates are not accessible by this synthetic route. Therefore, modified reaction schemes were tried using a stronger base, different metal salts, different reactant ratio, and altered sequence of addition. Finally, $Ln(NO_3)_3/Co(OAc)_2/H_2vab/NaOMe$ in a 0.4:0.5:1:1 ratio in methanol followed by slow evaporation of the solvent afforded crystalline compounds of $Co^{II}_2Ln^{III}$ ($Ln^{III} = Nd^{III}, Sm^{III}, Gd^{III}, Tb^{III}, Dy^{III}$) 2–6. All of these reactions also yielded single crystals of a heptanuclear, homometallic Co^{II}_7 species, 7. This compound was separated manually, and the identity of the secondary compound also was established by single crystal X-ray diffraction studies.

The Schiff bases as N,O-donors are capable of forming multiple coordinate bonds with the metal ions through azomethine, as well as the phenolic, benzylic, and methoxy groups. The characteristic FT-IR band of the coordinated ligand and the counteranion are displayed in Figure S1 in the

Scheme 2. Synthetic Route of Complexes 1–7



Supporting Information. In the FT-IR spectrum, strong and sharp bands due to the azomethine $\bar{\nu}$ (C=N) of free H₂vab is observed at 1618 cm⁻¹. In 1–7, this band is shifted to lower frequency and appears at 1608–1614 cm⁻¹, indicating a decrease in the C=N bond order due to the bond formation between Co^{II} and the imine nitrogen lone pair of the Schiff base. It is consistent with the X-ray diffraction results obtained for 1–7. The metal–nitrogen and metal–oxygen bonds are also confirmed by the new bands in the spectra of the complexes at 446–452 and 555–462 cm⁻¹, respectively, assigned in the low frequency region. The strong phenolic $\bar{\nu}$ (C–O) at 1259 cm⁻¹ in the free ligand is red-shifted due to coordination at 1230–1242 cm⁻¹. In the FTIR spectra of 2–7, the characteristic frequencies of nitrates appear at 1385 cm⁻¹. The broad IR absorption in the region 3391–3430 cm⁻¹ is attributed to the O–H stretching frequency of H₂O/MeOH molecules. In order to investigate the presence of heterometals, specifically in the representative heterometallic complex 3, and confirm the homogeneity of the crystals, energy dispersive X-ray spectroscopy (EDS) measurements were performed. The results confirm the presence of both Co and Tb (lanthanide) ions with a Co/Tb ratio 68.5:31.5 in corroboration with the results obtained from single crystal X-ray diffraction (shown in the Supporting Information, Figure S2). As the crystal qualities of 2 and 6 are not good enough, we have provided PXRD data to support the structures (Figure S3). In order to confirm the stability of the synthesized complex in solution, ESI–MS experiments were carried out in acetonitrile solvent. For complex 1, the molecular ion peak was observed at 1257.82 amu which corresponds to $[\{Co_4(vab)_4\} + H^+]^+$ (see Figure S4). For complex 7 two molecular ion peaks were observed: a $[Co_7(vab)_6]^{2+}$ core was observed at 971.545 amu (70%), while a hydrated core, $[Co_7(vab)_6 + H_2O]^{2+}$, appeared at 980.91 amu (Figure S5). The ESI–MS spectra of Co₂Tb displayed numerous fragmented peaks (see Figure S6). Close inspection of the spectrum shows removal of varying degrees of Co^{II}, NO₃⁻, and Hvab⁻ from the core of $[Co_2Tb(Hvab)_4(NO_3)]^{2+}$ giving rise to the multitude of observed peaks. The molecular integrity of the complex in solution was affirmed by the presence of the isotopic peak at 1363.14 amu, which corresponds to $[Co_2Tb(Hvab)_3(vab)(NO_3)]^+$. Isotopic peaks at 1300.003, 1243.01, 1102.86, and 1048.2 amu signify the species $[Co_2Tb(Hvab)_2(vab)_2]^+$, $[CoTb(Hvab)_4]^+$, $[Co_2Tb(Hvab)(vab)_2(NO_3)]^+$, and $[CoTb(Hvab)_3(NO_3)]^+$, respectively.

3.2. Structural Studies. X-ray crystallographic data reveal that 1 crystallizes in the tetragonal space group $I4_1/a$ with $Z = 4$. The molecular structure of 1 is shown in Figure 1, and the selected bond distances and angles are summarized in Table 1. The central motif of 1 is a cubane $[Co_4(\mu_3-O)_4]^{4+}$ core composed of two interconnected tetrahedrons of four Co^{II} centers and four μ_3 -O_{benzyl} atoms originating from four doubly deprotonated tridentate vab^{2-} utilizing the $\eta^1:\eta^1:\eta^3:\mu_3$ coordination mode, respectively (see Figure S7 and Scheme 1). The asymmetric unit of 1 contains quarter of the molecule along with one tetrahydrofuran and one water solvent molecule of crystallization. The six coordination sites of Co^{II} ions are occupied by four oxygen atoms and one nitrogen atom from vab^{2-} and a water molecule results in distorted octahedral geometry (see Figures S8 and S9 and Tables S2a and S3).^{10,11} Three corners of the octahedron are occupied by the O-atoms from the benzylic arms of three vab^{2-} , which act as bridges to the remaining metal atoms within the cubane core. Other

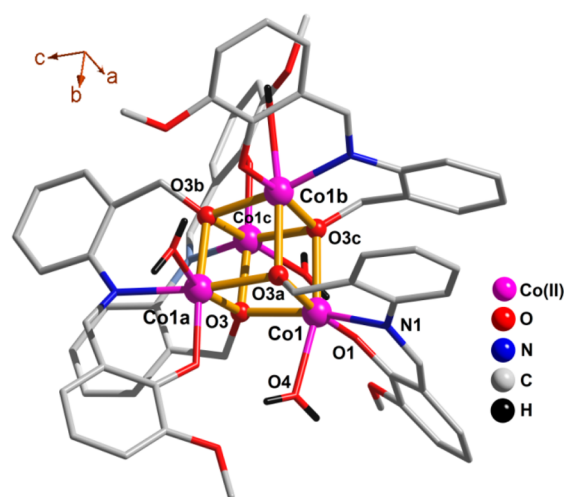


Figure 1. Molecular structure of 1 (hydrogen atoms, except those present in coordinated water molecule and solvent molecules of crystallization were omitted for clarity). Symmetry transformations used to generate equivalent atoms: $a = 5/4 - y, 1/4 + x, 5/4 - z; c = -1/4 + y, 5/4 - x, 5/4 - z$.

positions are occupied by phenolic–O and imine–N of the ligand and one O-atom of the exogenous water molecule. All the Co–O and Co–N bond lengths are in the range of 1.976(4)–2.250(5) Å and 2.105(5) Å, respectively; the Co–O_{water} bond length being the longest (2.250(5) Å). The charge balance and the bond lengths confirm that the metal centers are in the +2 oxidation state and the protonation level of the μ_3 -O atoms is as OR⁻ atoms, which is also in accord with the bond valence sum (BVS) analysis (see Table S4 and Table S5).¹² An interesting feature of 1 is the stabilization of the cubane core by intramolecular hydrogen bonds between the exogenous H₂O molecules and the O_{phenolate} (see Figure S10 and Table S6). The structural cohesion is ascribed to weak C–H \cdots π interactions (3.4–4.1 Å) between methoxy carbon C7 of *o*-vanillin to the benzylic π planes of the adjacent molecules, as shown in the packing diagram (see Figure S11).¹³ The structural features of 1 are similar to the previously published Co^{II}₄ compounds.¹⁴

Single crystal X-ray diffraction reveals that complexes 2–6 crystallize in the triclinic system, and according to the observed systematic extinctions, their structures were solved in the $P\bar{1}$ space group with $Z = 2$. As complexes 2–6 are isostructural, the structure of 5 is described in detail as a representative example. The structural details of all the other compounds are given in the Supporting Information (Figures S12–S15 and Tables S7–S10).

The crystal structure the dicationic heterometallic trinuclear $[Co_2Tb(Hvab)_4(NO_3)]^{2+}$ cluster consists of one Tb^{III} ion, two Co^{II} ions, four Hvab²⁻ ligands, and one coordinated nitrito ligand along with two nitrate counteranions and two lattice solvent molecules as shown in Figure 2. The important geometrical parameters of 5 are tabulated in Table 2. The central nonplanar $[Co_2Tb(\mu_2-O)_4]^{3+}$ core surrounded by four Hvab⁻ ligands, utilizes the $\eta^1:\eta^2:\eta^1:\eta^1:\mu_2$ coordination mode and is capped by a nitrate ion from one side (Scheme 1). Each tetradentate Hvab⁻ ligand connects Co^{II} and Tb^{III}, the O_{benzylic} and N_{imine} coordinates exclusively to the Co^{II} center, while the O_{methoxy} binds to Tb^{III}, and O_{phenolate} bridges Co^{II} and Tb^{III}. The oxidation states of the cobalt ions and the assignment of the protonation level of the coordinated oxygen atoms in Hvab⁻ were performed by inspection of the metric parameters,

Table 1. Selected Geometrical Parameters (Distances/Å and Angles/deg) for 1^a

Co1–O1	1.1976(4)	Co1–O3	2.125(3)
Co1–O4	2.250(5)	Co1–O3a	2.024(3)
Co1–N1	2.105(5)	Co1–O3c	2.157(3)
Co1...Co1a	3.1200(10)	Co1a...Co1c	3.2416(11)
Co1–O3–Co1a	93.55(12)	Co1a–O3–Co1c	101.63(14)
Co1–O3–Co1c	97.52(13)	O3–Co1–N1	169.18(15)

^aSymmetry transformations used to generate equivalent atoms: a = 5/4 – y, 1/4 + x, 5/4 – z; c = –1/4 + y, 5/4 – x, 5/4 – z.

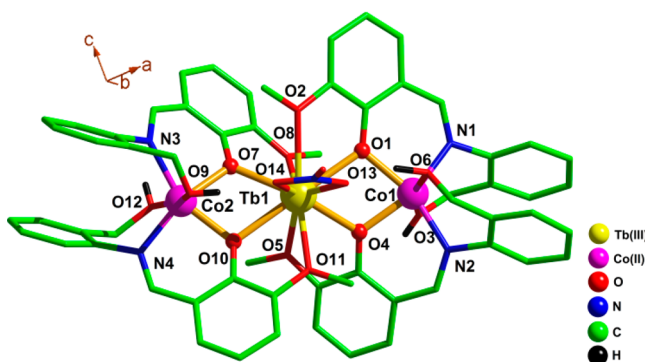


Figure 2. Molecular structure of 5 (all the hydrogen atoms except those present in coordinated benzylic oxygen atoms, counteranions, and the solvent molecules of crystallization were omitted for clarity).

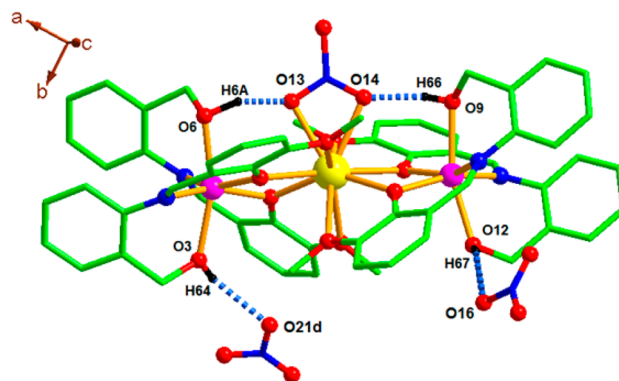


Figure 3. Intra- and intermolecular hydrogen bonding in complex 5. Symmetry transformations used to generate equivalent atoms: d = x, 1 + y, z.

charge-balance considerations, and BVS analysis (see Tables S4 and S5). A structural examination of the core reveals the presence of two puckered $\text{CoTb}(\text{O}_{\text{phenolate}})_2$ units with a dihedral angle 21.54° (α) and 21.67° (β) connected via central Tb^{III} in a twisted manner resulting in a nearly linear $\text{Co}^{\text{II}}-\text{Tb}^{\text{III}}-\text{Co}^{\text{II}}$ arrangement (170.68°) with average an $\text{Co}-\text{Tb}$ distance of 3.62 \AA (see Table 2). The two least-squares planes defined by $\text{CoTb}(\text{O}_{\text{phenolate}})_2$ units maintain a dihedral angle of 30.30° (γ) (see Figure S16). As shown in Figure 3, both Co1 and Co2 show six-coordinated distorted geometry composed of N_{imine} (av. 2.04 \AA), $\text{O}_{\text{phenolate}}$ (av. 2.04 \AA), and $\text{O}_{\text{benzylic}}$ (av. 2.2 \AA). The Tb1 ion is surrounded by $\text{O}_{\text{phenolate}}$ and $\text{O}_{\text{methoxy}}$ of the four Hvab^- ligands and capped by a $\eta^1:\eta^1:\mu_2$ nitrito ligand to create a distorted 10-coordinate polyhedral geometry. The three types of $\text{Tb}-\text{O}$ bond lengths of av. 2.62 \AA (for $\text{Tb}-\text{O}_{\text{methoxy}}$), av. 2.44 \AA (for $\text{Tb}-\text{O}_{\text{nitro}}$), and 2.40 \AA (for $\text{Tb}-\text{O}_{\text{phenolate}}$) are in typical range of $\text{Ln}-\text{O}$ distances. Continuous

shape measurement analyses reveal (see Tables S2a and S2b) that the actual polyhedral shape for cobalt center appears to be in between an octahedron (O_h) and a trigonal prism (D_{3h}), while for the terbium center a bicapped square antiprism (D_{4d}) and a sphenocorona (C_{2v}), delineate the experimental shape (see Figure S8). Interestingly, the four protonated benzylic oxygen atoms are actively engaged in hydrogen bonding with coordinated and noncoordinated nitrate groups. As shown in Figure 3, 5 possesses an intra-molecular moderately strong hydrogen bonding involving capping nitrate and two $\text{O}_{\text{benzylic}}$ (av. 2.73 \AA), while the other two $\text{O}_{\text{benzylic}}$ form intermolecular hydrogen bonding with counteranions (Table S6). The closest intermolecular distance between Tb1 ions in the supra-molecular assembly is 11.995 \AA with significant $\text{C}-\text{H}\cdots\pi$ interactions between neighboring molecules in the crystal packing as shown in Figure S17.

Table 2. Selected Geometrical Parameters (Distances/Å and Angles/deg) for 5^a

Co1–O1	2.051(4)	Tb1–O1	2.457(5)	Co2–O7	2.042(5)
Co1–O3	2.245(5)	Tb1–O4	2.323(5)	Co2–O9	2.226(5)
Co1–O4	2.020(6)	Tb1–O7	2.316(5)	Co2–O10	2.033(4)
Co1–O6	2.194(5)	Tb1–O10	2.505(5)	Co2–O12	2.218(6)
Co1–N1	2.042(6)	Tb1–O2	2.615(5)	Co2–N3	2.072(5)
Co1–N2	2.083(5)	Tb1–O5	2.600(5)	Co2–N4	2.044(7)
		Tb1–O8	2.619(5)		
		Tb1–O11	2.651(4)		
		Tb1–O13	2.446(5)		
		Tb1–O14	2.443(5)		
Co1...Tb1	3.626	Co1...Co2	7.228	Co2...Tb1	3.626
Co1–O1–Tb1	106.75(17)	Co1–Tb1–Co2	170.68	Co2–O7–Tb1	112.45(18)
Co1–O4–Tb1	113.1(2)			Co2–O10–Tb1	105.57(17)
Co1–O2–Tb1(α)	21.54	Co2–O2–Tb1(β)	21.67	Co1 Tb1O2–Co2 Tb1O2(γ)	30.30

^aDihedral angle, α = angle between Co1O1Tb1 and Co1O4Tb1 planes; β = angle between Co1O7Tb1 and Co2O10Tb1 planes; γ = dihedral angle between two CoTbO_2 square planes

Table 3. Structural and Magnetic features of Co^{II}₂Ln^{III}Assemblies^a

complex	Co ^{II} ...Ln ^{III} (Å)	Co ^{II} ...Co ^{II} (Å)	Co ^{II} ...Ln ^{III} ...Co ^{II} (deg)	local geometry of Ln ^{III} center	magnetism	ref
[Co ₂ Gd(L ¹) ₂].NO ₃ .2CHCl ₃	3.307	6.614	180	12-coordinated, distorted icosahedrons	SMM	3a
[Co ₂ Tb(L ¹) ₂].NO ₃ .2CHCl ₃	3.331	6.621	180	12-coordinated, distorted icosahedrons	SMM	3b
[Co ₂ Dy(L ¹) ₂].NO ₃ .2CHCl ₃	2.281	6.652	180	12-coordinated, distorted icosahedrons	SMM	3b
[Co ₂ Ho(L ¹) ₂].NO ₃ .2CHCl ₃	3.269	6.654	180	12-coordinated, distorted icosahedrons	SMM	3b
[Co ₂ Eu(L ¹) ₂].Cl.2CHCl ₃	3.331–3.339	6.669	177.48	12-coordinated, distorted icosahedrons	non SMM	3b
[Co ₂ Gd(L ²) ₂].NO ₃ .3CH ₃ OH	3.313–3.322	6.634	178.41	8-coordinated	SMM	3c
[Co ₂ Tb(L ²) ₂].NO ₃ .3CH ₃ OH	3.331	6.662	107.23			
[Co ₂ Dy(L ²) ₂].NO ₃ .3CH ₃ OH	3.302–3.303	6.604	177.86	8-coordinated	SMM	3c
[Co ₂ Dy(L ²) ₂].NO ₃ .3CH ₃ OH	3.306	6.612	178.42			
[Co ₂ Dy(L ²) ₂].NO ₃ .3CH ₃ OH	3.301–3.304	6.606	178.2	8-coordinated	SMM	3c
[Co ₂ Nd(piv) ₆ (C ₉ H ₇ N) ₂ (NO ₃) ₂]	4.067–4.070	7.493	134.10	8-coordinated, distorted dodecahedron	antiferromagnetic	4a
[Co ₂ Nd(piv) ₆ (C ₉ H ₇ N) ₂ (NO ₃) ₂]	4.067–4.070	7.493	134.10	8-coordinated, distorted dodecahedron	ferromagnetic	4b
[Co ₂ La(L ³) ₂ (H ₂ O) ₄][Cr(CN) ₆] ₂ .nH ₂ O	3.693–3.722	7.368	167.12	10-coordinated	antiferromagnetic	4c
[Co ₂ Gd(L ³) ₂ (H ₂ O) ₄][Cr(CN) ₆] ₂ .nH ₂ O	3.667	7.323	173.42	10-coordinated	ferromagnetic	4c
[Co ₂ Tb(μ ₃ -OH)(nic) ₅ (N ₃) ₂]	3.396–3.693	3.812	64.91	7-coordinated monocappedtriagonal prism	ferromagnetic	4d
[Co ₂ Gd(μ ₃ -OH)(nic) ₅ (N ₃) ₂]	3.409–3.699	3.810	64.67	7-coordinated monocappedtriagonal prism	ferromagnetic	4d
[Co ₂ Dy(μ ₃ -OH)(nic) ₅ (N ₃) ₂]	3.326–3.627	3.810	65.02	7-coordinated monocappedtriagonal prism	ferromagnetic	4d
[Co ₂ Eu(μ ₃ -OH)(nic) ₅ (N ₃) ₂]	3.419–3.703	3.808	64.49	7-coordinated monocappedtriagonal prism	ferromagnetic	4d
[Co ₂ Sm(μ ₃ -OH)(nic) ₅ (N ₃) ₂]	3.429–3.702	3.803	64.33	7-coordinated monocappedtriagonal prism	ferromagnetic	4d
[Co ₂ Nd(Hvab) ₄ (NO ₃) ₂](NO ₃) ₂ (2)	3.669	7.316	170.94	10-coordinated	antiferromagnetic	this work
[Co ₂ Sm(Hvab) ₄ (NO ₃) ₂](NO ₃) ₂ (3)	3.632–3.636	7.246	170.98	10-coordinated	SMM	this work
[Co ₂ Gd(Hvab) ₄ (NO ₃) ₂](NO ₃) ₂ (4)	3.648–3.651	7.274	170.60	10-coordinated	SMM	this work
[Co ₂ Tb(Hvab) ₄ (NO ₃) ₂](NO ₃) ₂ (5)	3.626	7.228	170.68	10-coordinated	weak SMM	this work
[Co ₂ Dy(Hvab) ₄ (NO ₃) ₂](NO ₃) ₂ (6)	3.631	7.239	170.71	10-coordinated	weak SMM	this work

^aAbbreviation: H₃L¹ = (S)P[N(Me)N=CH-C₆H₃-2-OH-3-OMe]₃, H₃L² = N,N',N''-tris(2-hydroxy-3-methoxybenzylidene)-2-(aminomethyl)-2-methyl-1,3-propanediamine, Hpiv = pivalic acid, H₂L³ = 2,6-di(acetoacetyl)pyridine, Hnic = nicotinic acid.

It is interesting to compare the trinuclear Co^{II}₂Ln^{III} core of the current members with those reported in the literature compiled in Table 3. In its essential features, if we consider only the phenolate/enolate bridged species, the structural pattern of 2–6 could be related to only four previous reports.^{3a–c,4c} A close scrutiny of the previous reports reveals the following characteristics: (i) Ohba and co-workers utilized 2,6-di(acetoacetyl)pyridine to construct Co^{II}₂Ln^{III} core where each Co^{II}–Ln^{III} connection was established by two enolate bridges.^{4c} (ii) Chandrasekhar et al. published two reports exploiting a tripodal, phosphorus-based tris hydrazone ligand containing vanillin moiety, L¹H₃, which results in triple phenolate bridged Co^{II}–Ln^{III} connectivity displaying SMM behavior.^{3a,b} (iii) Following similar synthetic consideration of using a vanillin-based tripodal ligand in 2010,^{3c} Wernsdorfer and co-workers used N,N',N''-tris(2-hydroxy-3-methoxybenzylidene)-(aminomethyl)-2-methyl-1,3-propanediamine to generate a series of Co^{II}₂Ln^{III} cores where Co^{II} and Ln^{III} are connected by means of triple phenolate bridge and exhibit characteristics like SMM.

If we further streamline these observations, it could be said that only two different ligand systems have been used to date to generate an enolate/phenolate bridged Co^{II}₂Ln^{III} assembly, namely, acetoacetylpyridine^{4c} and vanillin containing tripodal ligands^{3a–c} of which the last category of ligand system promotes SMM behavior in the resulting compounds.

We have utilized a nontripodal vanillin containing a Schiff base ligand which spans its coordinating activity by nesting Co^{II} in a N_{pyridine}/O_{phenolate} pocket and Ln^{III} in an O_{phenolate}/O_{methoxy} pocket. Here, Co^{II} and Ln^{III} are connected via two O_{phenolate} resulting in a near planar CoLnO₂ diamond like core. In terms of magnetic properties (*vide infra*), it is only the third ligand system that builds Co^{II}₂Ln SMMs (Table 3).

X-ray crystallography reveals that the centrosymmetric wheel-shaped heptanuclear cluster having the general formula [Co^{II}₇(vab)₆](NO₃)₂.2H₂O crystallized in P2₁/c with Z = 2. The asymmetric unit comprises four crystallographically independent cobalt ions (Co1, Co2, Co3, and Co4) with three independent vab²⁻ ligands along with one counter nitrate anion and water solvent molecule. The molecular structure of 7

is shown in Figure 4, and the selected bond distances and angles are summarized in Table 4. Three symmetry related

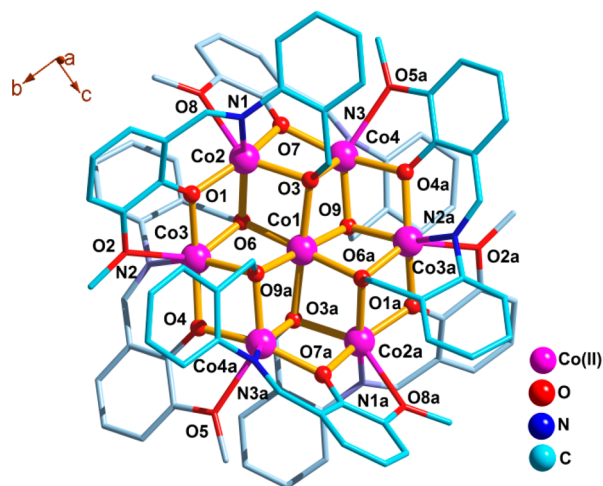


Figure 4. Molecular structure of **7** (all the hydrogen atoms, counter anions, and the solvent molecules of crystallization were omitted for clarity). Symmetry transformations used to generate equivalent atoms: $a = 1 - x$, $1 - y$, $1 - z$.

Co2–Co2a, Co3–Co3a, and Co4–Co4a pairs associated with central Co1 are ligated by six μ_2 -O_{phenolate} and six μ_3 -O_{benzylic} to give a $[\text{Co}^{\text{II}}_7(\mu_2\text{-O})_6(\mu_3\text{-O})_6]^{2+}$ core with the nearest Co...Co distance of 3.099 Å. It can also be visualized as six distorted missing-corner cubanes sharing the neighboring faces of one another as shown in the Supporting Information (Figure S18). All cobalt atoms are assigned as Co^{II} ions, and μ_3 -O and μ_2 -O atoms as OR⁻ atoms as revealed by the BVS calculated results and charge balance considerations (Tables S3 and S4). The six doubly deprotonated vab²⁻ ligands bridge the six outer Co^{II} ions via the $\eta^1:\eta^2:\eta^1:\eta^3:\mu_4$ binding motif (see Scheme 1) and sit alternately above and below the $\{\text{Co}^{\text{II}}_7(\mu_2\text{-O})_6(\mu_3\text{-O})_6\}^{2+}$ plane. The coordination sphere of the central cobalt ion (Co1) consists of six oxygen atoms from the benzylic arms of vab²⁻ ligands and connects the central cobalt ion to the outer cobalt ions in a μ_3 -O_{benz} fashion (Co1–O_{benzylic} = 2.105(5)–2.148(5) Å (Figures S8 and S9 and Tables S2a and S3). Each cobalt ion situated on the rim is coordinated with two O_{benzylic}, two O_{phenolate} (Co–O = 1.984(5)–2.438 Å), one N_{imino} (Co–N = 2.061(6)–2.074(6) Å), and weakly coordinated O_{methoxo} (Co...

O_{methoxo} = 2.415–2.438 Å) of vab²⁻ in a highly distorted geometry between octahedron and trigonal prism (Table S2a). The peripheral cobalt centers are connected by the μ_2 -O_{phenoxo}. The core of the cluster can be described as an almost planar Co₆ moiety with a crystallographically imposed S₂-symmetry with adjacent Co...Co distances of 3.099–3.195 Å. A 2D supramolecular architecture is assembled by the propagation of multiple interactions between the NO₃⁻ counteranions and the individual $[\text{Co}^{\text{II}}_7(\text{vab})_6]$ moieties in the crystal packing (see Figures S19 and S20 and Table S6). This type of Co^{II}₇ core structure has already been encountered in the literature.¹⁵

3.3. Magnetic Studies. dc Magnetic Susceptibility Studies. dc magnetic susceptibility data on microcrystalline powdered samples **1–7** were recorded in the temperature range of 5.0–300 K, using an applied field of 0.1 T. The sample was restrained in eicosane to prevent torquing.

Figure 5 shows the plot of $\chi_M T$ vs T for complex **1**. The $\chi_M T$ for **1** remains constant at a value of approximately 13.70 cm³ mol⁻¹ K at 300 K down to 60 K before it steadily decreases to a value of 10.05 cm³ mol⁻¹ K at 5.0 K, indicating the presence of antiferromagnetic exchange interactions between the metal centers at lower temperature. The $\chi_M T$ value at 300 K is higher than the predicted spin-only ($g = 2.00$) value of 7.5 cm³ mol⁻¹ K expected for four noninteracting Co²⁺ ions; this is likely due to the unquenched spin orbital angular momentum observed for octahedral Co²⁺ ions. The decrease in $\chi_M T$ with decreasing temperature indicates antiferromagnetic interactions over the entire temperature range. Figure 5 shows the plot of $\chi_M T$ vs T for complexes **2–6**. The $\chi_M T$ for **2** steadily decreases from a value of 7.01 cm³ mol⁻¹ K from 300 K to a value 4.65 cm³ mol⁻¹ K at 5 K, indicating predominant antiferromagnetic interactions between the metal centers. The $\chi_M T$ for **3** remains fairly constant at a value of 6.15 cm³ mol⁻¹ K from 300 to 120 K before slightly decreasing to a value of 5.11 cm³ mol⁻¹ K at 20 K and then slowly increasing to a value of 6.30 cm³ mol⁻¹ K at 5 K, indicating the presence of antiferromagnetic interactions at higher temperatures before ferromagnetic interactions are observed at low temperatures. The $\chi_M T$ for **4** steadily increases with decreasing temperature from 14.19 cm³ mol⁻¹ K at 300 K to 15.21 cm³ mol⁻¹ K at 40 K, before dramatically increasing to a value of 23.67 cm³ mol⁻¹ K at 5.0 K. The $\chi_M T$ value at 300 K is higher than the predicted spin-only ($g = 2.00$) value of 11.625 cm³ mol⁻¹ K expected for two noninteracting Co²⁺ and one noninteracting Gd³⁺ ion indicating the presence of predominant ferromagnetic exchange interactions between the metal

Table 4. Selected Geometrical Parameters (Distances/Å and Angles/deg) for **7**^a

Co1–O3	2.148(5)	Co2–O8	2.438	Co3–N2	2.061(6)
Co1–O6	2.105(5)	Co2–N1	2.071(6)	Co4–O3	2.178(5)
Co1–O9	2.109(5)	Co3–O1	2.033(5)	Co4–O4a	2.037(5)
Co2–O1	1.993(5)	Co3–O2	2.413	Co4–O5a	2.415
Co2–O3	2.039(5)	Co3–O4	1.984(5)	Co4–O7	2.003(5)
Co2–O6	2.168(5)	Co3–O6	2.047(5)	Co4–O9	2.048(5)
Co2–O7	2.053(5)	Co3–O9a	2.170(5)	Co4–N3	2.074(6)
Co1...Co2	3.118	Co1...Co4	3.125	Co2...Co4	3.195
Co1...Co3	3.099	Co2...Co3	3.184	Co3...Co4a	1.191
Co1–O6–Co2	93.72(18)	Co1–O9–Co4	97.5(2)	Co2–O1–Co3	104.6(2)
Co1–O3–Co2	96.2(2)	Co1–O3–Co4	92.48(19)	Co2–O6–Co3	98.11(18)
Co1–O6–Co3	96.54(18)	Co2–O7–Co4	104.0(2)	Co3–O4–Co4a	105.0(2)
Co1–O9a–Co3	92.8(2)	Co2–O3–Co4	98.5(2)	Co3–O9–Co4a	98.3(2)

^aSymmetry transformations used to generate equivalent atoms: $a = 1 - x$, $1 - y$, $1 - z$.

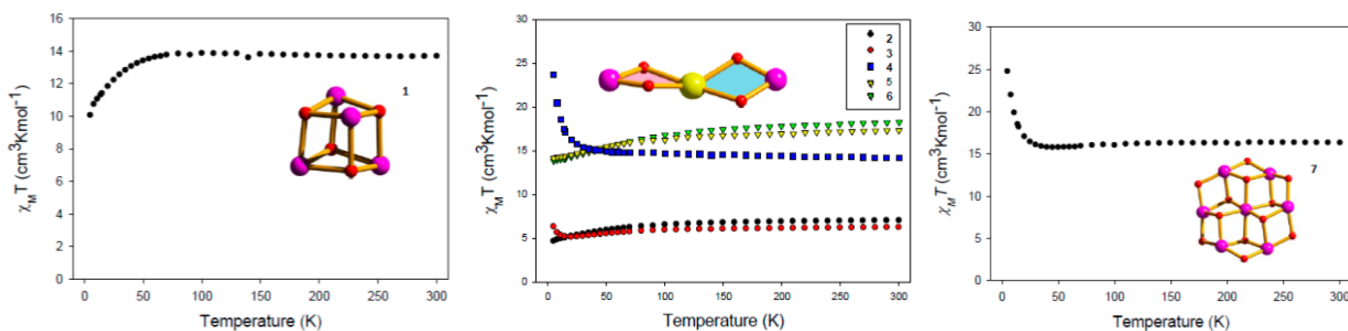


Figure 5. $\chi_M T$ vs T plot for complexes 1–7 in a 1000 G *dc* field.

centers over the entire temperature range. The $\chi_M T$ for 5 slightly decreases with decreasing temperature from $17.30 \text{ cm}^3 \text{ mol}^{-1} \text{ K}$ at 300 K down to $14.13 \text{ cm}^3 \text{ mol}^{-1} \text{ K}$ at 5.0 K, indicating the presence of antiferromagnetic interactions between the metal centers. The $\chi_M T$ for 6 slightly decreases with decreasing temperature from $18.24 \text{ cm}^3 \text{ mol}^{-1} \text{ K}$ at 300 K down to $13.82 \text{ cm}^3 \text{ mol}^{-1} \text{ K}$ at 5.0 K, suggesting the presence of antiferromagnetic interactions.

Figure 5 shows the plot of $\chi_M T$ vs T for complex 7. The $\chi_M T$ for 7 remains fairly constant at a value of approximately $16.29 \text{ cm}^3 \text{ mol}^{-1} \text{ K}$ at 300 K down to 25 K before it dramatically increases to a value of $24.73 \text{ cm}^3 \text{ mol}^{-1} \text{ K}$ at 5.0 K, indicating the presence of ferromagnetic exchange interactions between the metal centers at lower temperature. The $\chi_M T$ value at 300 K is higher than the predicted spin-only ($g = 2.00$) value of $13.125 \text{ cm}^3 \text{ mol}^{-1} \text{ K}$ expected for seven noninteracting Co^{2+} ions; this is likely due to the unquenched spin orbital angular momentum observed for octahedral Co^{2+} ions.

ac Magnetic Susceptibility Studies. As a result of the notable single-ion anisotropy of the lanthanide ions and unquenched spin orbital angular momentum of the Co^{2+} ions, *ac* susceptibility studies were carried out on complexes 1–7 in the 1.8–15 K region in zero applied field with a 3.5 Oe driving field to probe for slow magnetic relaxation, i.e., SMM behavior. The *ac* in-phase susceptibility studies of complex 1, shown as $\chi'_M T$ vs T in Figure S21, were collected at various frequencies. The values at high temperatures agree well with the *dc* susceptibility data at the same temperature. The in-phase susceptibility displays features similar to the *dc* plot, further suggesting the depopulation of excited states as temperature is lowered and at low temperature displays a slight frequency dependent drop. The out-of-phase susceptibility (χ''_M , Figure 6) shows a slight tail at low temperatures, indicating 1 might display behavior characteristic of a weak SMM.

The *ac* in-phase susceptibility for complex 2 ($\chi'_M T$ vs T , Figure S22) shows a slight decrease with decreasing temperature and is in good agreement with the *dc* susceptibility data. However, no frequency dependent drop is seen in the in-phase susceptibility for complex 2 at low temperatures, and consequently no signal is observed in the *ac* out-of-phase susceptibility (χ''_M , Figure S23), indicating complex 2 does not display behavior characteristic of a SMM. The *ac* in-phase susceptibility of complex 3 ($\chi'_M T$ vs T , Figure S24) is in good agreement with the *dc* data at the same temperature range and similarly to 3 continues to show an increase in $\chi'_M T$ with decreasing temperatures before a slight frequency dependent drop is observed at low temperature. Also similarly to 3, a frequency dependent rise in the out-of-phase susceptibility (χ''_M , Figure 7) is observed as a peak tail, indicating 3 also

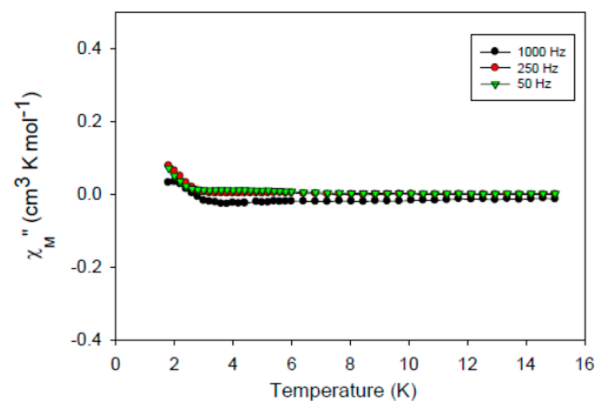


Figure 6. Plot of χ''_M signal for dried, microcrystalline complex 1 at the indicated frequencies.

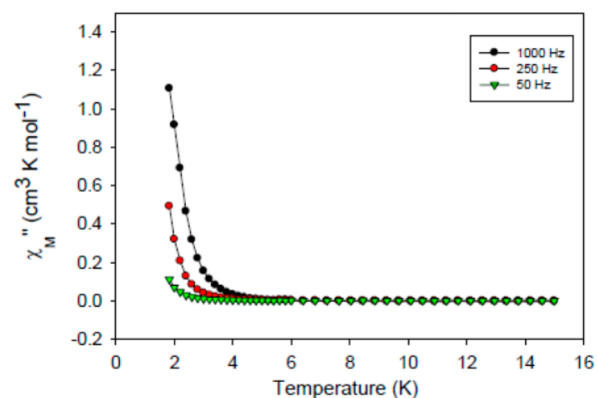


Figure 7. Plot of χ''_M signal for dried, microcrystalline complex 3 at the indicated frequencies.

displays behavior characteristic of a SMM. The *ac* in-phase susceptibility of complex 4 ($\chi'_M T$ vs T , Figure S25) is in good agreement with the *dc* data at the same temperature range and continues to show an increase in $\chi'_M T$ with decreasing temperatures before a slight frequency dependent drop is observed at low temperature. Consequently, a frequency dependent rise in the out-of-phase susceptibility (χ''_M , Figure 8) is observed as a peak tail, indicating 4 also displays behavior characteristic of a SMM. The *ac* in-phase susceptibility ($\chi'_M T$ vs T , Figure S26) of complex 5 is in good agreement with the *dc* data at the same temperature and relatively flat indicating the presence of very few low-lying excited states. There is the slight beginning of peak tail in the out-of-phase (χ''_M , Figure S27), indicating 5 also displays behavior characteristic of a weak SMM. The *ac* in-phase susceptibility ($\chi'_M T$ vs T , Figure S28) of

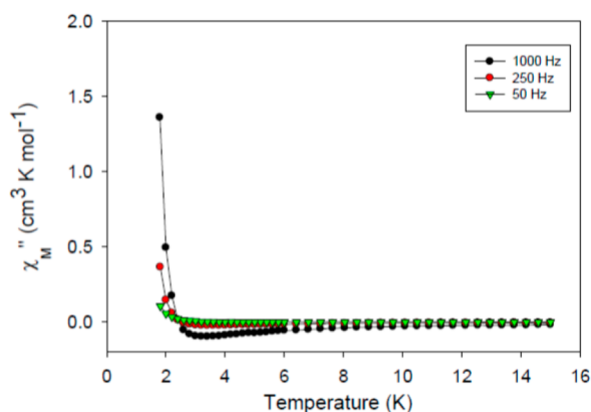


Figure 8. Plot of χ''_M signal for dried, microcrystalline complex 4 at the indicated frequencies.

complex 6 is in good agreement with the *dc* data at the same temperature and is relatively flat, indicating the presence of very few low-lying excited states. There is the slight beginning of peak tail in the out-of-phase (χ''_{Mv} Figure S29), indicating 6 displays behavior characteristic of a weak SMM.

The *ac* in-phase susceptibility studies of complex 7, shown as $\chi'_M T$ vs *T* in Figure 9 were collected at various frequencies. The

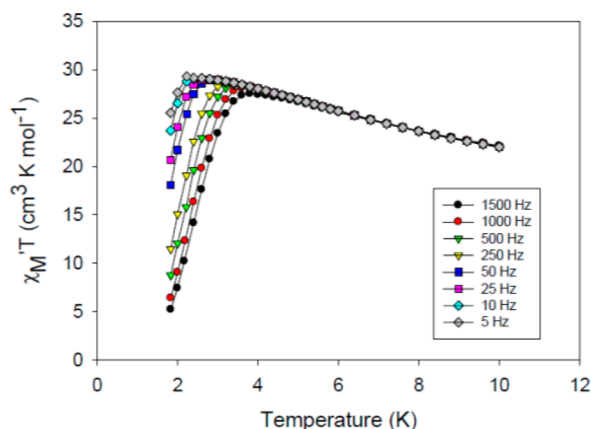


Figure 9. Plot of $\chi'_M T$ signal for dried, microcrystalline complex 7 at the indicated frequencies.

values at high temperatures agree with the *dc* susceptibility data at the same temperature. The in-phase susceptibility measurements display features similar to the *dc* plot, including the increase in $\chi'_M T$ at low temperatures before a frequency dependent drop in the signal is observed around 4 K. The out-of-phase susceptibility (χ''_{Mv} Figure 10) shows a partial peak at frequencies greater than 500 Hz and tails for all the lower frequency suggesting 7 might display behavior characteristic of a slow magnetic relaxation and consequently SMM behavior.

In order to obtain an estimate of U_{eff} and τ_0 for 7 in the absence of χ''_M peak in *T* vs frequency data, we have used the χ'_M and χ''_M for the tails at four frequencies (ν) and at different *T* values to construct a $\log(\chi''_M/\chi'_M)$ vs $1/T$ plot (Figure 11) based on the Kramers–Kronig eq (eq 1),¹⁶ where $\omega (= 2\pi\nu)$ is the angular frequency of the *ac* field. Fitting of the data and

$$\log \frac{\chi''_M}{\chi'_M} = \log(\omega\tau_0) + \frac{U_{\text{eff}}}{k_B T} \quad (1)$$

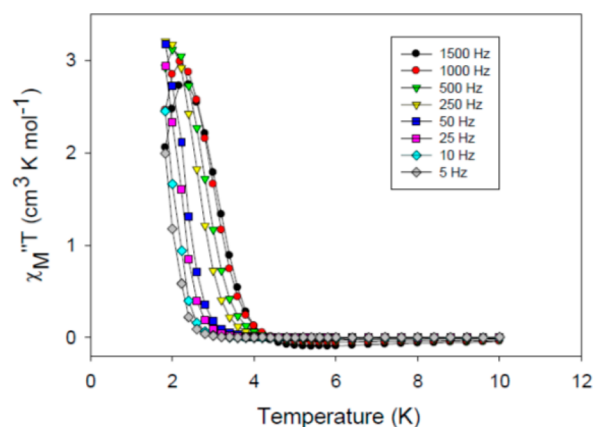


Figure 10. Plot of $\chi''_M T$ signal for dried, microcrystalline complex 7 at the indicated frequencies.

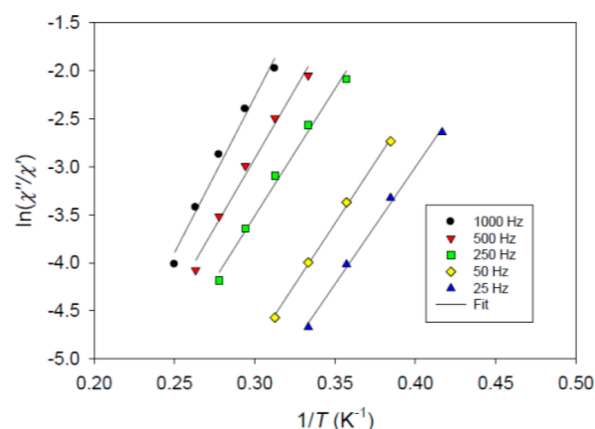


Figure 11. Plot of $\ln(\chi''_M/\chi'_M)$ vs $1/T$ for 7 in zero-applied field at the indicated *ac* frequencies. The solid lines are fits of the data; see the text for the fit parameters.

averaging of the obtained parameters gave $U_{\text{eff}} \approx 18.8 \pm 1.8 \text{ cm}^{-1}$ and $\tau_0 \approx 8.9 \pm 0.6 \times 10^{-9} \text{ s}$.

4. CONCLUSION

In summary, Co^{II}_4 1, a series of $\text{Co}^{\text{II}}_2\text{Ln}^{\text{III}}$ ($\text{Ln}^{\text{III}} = \text{Nd}^{\text{III}}$ 2, Sm^{III} 3, Gd^{III} 4, Tb^{III} 5, Dy^{III} 6) and Co^{II}_7 7, complexes were synthesized and structurally characterized. Of the two synthetic routes tested, the first one yielded only Co^{II}_4 cubane species. The synthetic route that produces $\text{Co}^{\text{II}}\text{--Ln}^{\text{III}}$ involves the combination of $\text{Ln}(\text{NO}_3)_3 \cdot x\text{H}_2\text{O}/\text{Co}(\text{OAc})_2/\text{H}_2\text{vab}/\text{NaOMe}$ in 0.4:0.5:1:1 ratio in methanol. This procedure also generates a heptanuclear homometallic Co_7 compound. Compounds 2–6 are the fifth reported complexes containing phenolate/enolate bridged $\text{Co}^{\text{II}}_2\text{Ln}^{\text{III}}$ core. Six of the reported complexes, 1, 3, 4, 5, 6, and 7, afford slow relaxation of magnetization and consequently SMM behavior. The contribution of the Ln^{III} ion is evidenced by the different magnetic behavior observed in the various $\text{Co}^{\text{II}}_2\text{Ln}^{\text{III}}$ compounds. Thus, the foregoing results illustrate how $\text{Co}^{\text{II}}\text{--Ln}^{\text{III}}$ systems can provide a successful platform to generate SMMs. At the same time, the study highlights the need for more detailed understanding on various factors that influence the magnetic outcome, opening up the route for yet to be explored synthetic strategies.

■ ASSOCIATED CONTENT

Supporting Information

The Supporting Information is available free of charge on the ACS Publications website at DOI: 10.1021/acs.inorgchem.6b01402.

FT-IR, EDX spectrum, PXRD, HR-ESI-MS spectrum, crystal data, crystal packing diagram, supramolecular interactions, Stiefel and Brown nomenclature, continuous shape measurement (CShM) results, BVS calculation results, metric parameter and additional magnetic data (PDF)

Crystallographic CIF files (CCDC 1483752–1483758) (CIF1, CIF2, CIF3, CIF4, CIF5, CIF6, CIF7)

■ AUTHOR INFORMATION

Corresponding Authors

*E-mail: christou@chem.ufl.edu (G.C.).

*E-mail: sgchem@caluniv.ac.in (S.G.).

Notes

The authors declare no competing financial interest.

■ ACKNOWLEDGMENTS

R.M and Y.S. acknowledge UGC, India, for RFSMS fellowship (Sanction No. UGC/740/RFSMS) and DST India (Sanction No. (SR/FT/CS-107/2011) respectively for financial support. DST-FIST and DST-Purse is gratefully acknowledged for providing the X-ray diffraction and HRMS facility at the Department of Chemistry, University of Calcutta.

■ REFERENCES

- (1) (a) Sessoli, R.; Gatteschi, D.; Caneschi, A.; Novak, M. A. Magnetic bistability in a metal-ion cluster. *Nature* **1993**, *365*, 141–143. (b) Slagereen, J. V. New directions in electron paramagnetic resonance spectroscopy on molecular nanomagnets. *Top. Curr. Chem.* **2011**, *321*, 199–234. (c) Gatteschi, D.; Sessoli, R. Quantum Tunneling of Magnetization and Related Phenomena in Molecular Materials. *Angew. Chem., Int. Ed.* **2003**, *42*, 268–297. (d) Bogani, L.; Wernsdorfer, W. Molecular spintronics using single-molecule magnets. *Nat. Mater.* **2008**, *7*, 179–186. (e) Vincent, R.; Klyatskaya, S.; Ruben, M.; Wernsdorfer, W.; Balestro, F. Electronic read-out of a single nuclear spin using a molecular spin transistor. *Nature* **2012**, *488*, 357–360.
- (2) (a) Rosado Piquer, L. R.; Sañudo, E. C. Heterometallic 3d–4f single-molecule magnets. *Dalton Trans.* **2015**, *44*, 8771–8780. (b) Winpenny, R. E. P. Quantum Information Processing Using Molecular Nanomagnets As Qubits. *Angew. Chem., Int. Ed.* **2008**, *47*, 7992–7994. (c) Murugesu, M.; Habrych, M.; Wernsdorfer, W.; Abboud, K. A.; Christou, G. Single-Molecule Magnets: A Mn₂₅ Complex with a Record S = 51/2 Spin for a Molecular Species. *J. Am. Chem. Soc.* **2004**, *126*, 4766–4767. (d) Sessoli, R.; Tsai, H.-L.; Schake, A. R.; Wang, S.; Vincent, J. B.; Folting, K.; Gatteschi, D.; Christou, G.; Hendrickson, D. N. High-spin molecules: [Mn₁₂O₁₂(O₂CR)₁₆(H₂O)₄]. *J. Am. Chem. Soc.* **1993**, *115*, 1804–1816. (e) Ako, A. M.; Hewitt, I. J.; Mereacre, V.; Clé rac, R.; Wernsdorfer, W.; Anson, C. E.; Powell, A. K. A Ferromagnetically Coupled Mn₁₉ Aggregate with a Record S = 83/2 Ground Spin State. *Angew. Chem., Int. Ed.* **2006**, *45*, 4926–4929. (f) Zheng, Y.-Z.; Evangelisti, M.; Winpenny, R. E. P. Large Magnetocaloric Effect in a Wells–Dawson Type {Ni₆Gd₆P₆} Ca. *Angew. Chem., Int. Ed.* **2011**, *50*, 3692–3695. (g) Moreno Pineda, E. M.; Tuna, F.; Pritchard, R. G.; Regan, A. C.; Winpenny, R. E. P.; McInnes, E. J. L. Molecular aminophosphonate cobalt–lanthanide clusters. *Chem. Commun.* **2013**, *49*, 3522–3524. (h) Woodruff, D. N.; Winpenny, R. E. P.; Layfield, R. A. Lanthanide Single-Molecule Magnets. *Chem. Rev.* **2013**, *113*, 5110–5148. (i) Benelli, C.; Gatteschi, D. Magnetism of Lanthanides in

Molecular Materials with Transition-Metal Ions and Organic Radicals. *Chem. Rev.* **2002**, *102*, 2369–2388.

- (3) (a) Chandrasekhar, V.; Pandian, B. M.; Azhakar, R.; Vittal, J. J.; Clerac, R. Linear Trinuclear Mixed-Metal Co^{II}–Gd^{III}–Co^{II} Single-Molecule Magnet: [L₂Co₂Gd][NO₃]₂·2CHCl₃ (LH₃ = (S)P[N(Me)N=CH–C₆H₃–2-OH–3-OMe]₃). *Inorg. Chem.* **2007**, *46*, 5140–5142. (b) Chandrasekhar, V.; Pandian, B. M.; Vittal, J. J.; Clerac, R. Synthesis, Structure, and Magnetism of Heterobimetallic Trinuclear Complexes {[L₂Co₂Ln][X]} [Ln = Eu, X = Cl; Ln = Tb, Dy, Ho, X = NO₃; LH₃ = (S)P[N(Me)N=CH–C₆H₃–2-OH–3-OMe]₃]: A 3d–4f Family of Single-Molecule Magnets. *Inorg. Chem.* **2009**, *48*, 1148–1157. (c) Yamaguchi, T.; Costes, J. P.; Kishima, Y.; Kojima, M.; Sunatsuki, Y.; Brefuel, N.; Tuchagues, J.-P.; Vendier, L.; Wernsdorfer, W. Face-Sharing Heterotrimeric M^{II}–Ln^{III}–M^{II} (M = Mn, Fe, Co, Zn; Ln = La, Gd, Tb, Dy) Complexes: Synthesis, Structures, and Magnetic Properties. *Inorg. Chem.* **2010**, *49*, 9125–9135. (d) Ruamps, R.; Batchelor, L. J.; Guillot, R.; Zakhia, G.; Barra, A.-L.; Wernsdorfer, W.; Guihery, N.; Mallah, T. Ising-type magnetic anisotropy and single molecule magnet behaviour in mononuclear trigonal bipyramidal Co(II) complexes. *Chem. Sci.* **2014**, *5*, 3418–3424. (e) Mondal, K. C.; Sundt, A.; Lan, Y.; Kostakis, G. E.; Waldmann, O.; Ungur, L.; Chibotaru, L. F.; Anson, C. E.; Powell, A. K. Coexistence of Distinct Single-Ion and Exchange-Based Mechanisms for Blocking of Magnetization in a Co^{II}₂Dy^{III}₂ Single-Molecule Magnet. *Angew. Chem., Int. Ed.* **2012**, *51*, 7550–7554. (f) Costes, J.-P.; Vendier, L.; Wernsdorfer, W. Structural and magnetic studies of original tetranuclear Co^{II}–Ln^{III} complexes (Ln^{III} = Gd, Tb, Y). *Dalton Trans.* **2011**, *40*, 1700–1706. (g) Zhao, X.-Q.; Lan, Y.; Zhao, B.; Cheng, P.; Anson, C. E.; Powell, A. K. Synthesis, structures and magnetic properties of a series of 3d–4f tetranuclear Co^{II}₂Ln^{III}₂ cubanes. *Dalton Trans.* **2010**, *39*, 4911–4917. (h) Wang, P.; Shannigrahi, S.; Yakovlev, N. L.; Hor, T. S. A. General One-Step Self-Assembly of Isostructural Intermetallic Co^{II}₃Ln^{III} Cubane Aggregates. *Inorg. Chem.* **2012**, *51*, 12059–12061. (i) Gomez, V.; Vendier, L.; Corbella, M.; Costes, J.-P. Tetranuclear [Co–Gd]₂ Complexes: Aiming at a Better Understanding of the 3d–Gd Magnetic Interaction. *Inorg. Chem.* **2012**, *51*, 6396–6404. (j) Sopasis, J. G.; Orfanoudaki, M.; Zampas, P.; Philippidis, A.; Siczek, M.; Lis, T.; O'Brien, J. R.; Milios, C. J. 2-Aminoisobutyric Acid in Co(II) and Co(II)/Ln(III) Chemistry: Homometallic and Heterometallic Clusters. *Inorg. Chem.* **2012**, *51*, 1170–1179. (k) Chandrasekhar, V.; Das, S.; Dey, A.; Hossain, S.; Lloret, F.; Pardo, E. Synthesis, Structure, and Magnetic Properties of a Family of Heterometallic Pentanuclear [Co₄Ln] (Ln = Gd^{III}, Dy^{III}, Tb^{III}, and Ho^{III}) Assemblies. *Eur. J. Inorg. Chem.* **2013**, *2013*, 4506–4514. (l) Orfanoudaki, M.; Tamiolakis, I.; Siczek, M.; Lis, T.; Armatas, G. S.; Pergantis, S. A.; Milios, C. Unique trigonal prism encapsulated Ln complexes: a [Co^{II}Eu] and a [Co^{II}Dy] cage. *J. Dalton Trans.* **2011**, *40*, 4793–4796. (m) Langley, S. K.; Chilton, N. F.; Moubaraki, B.; Murray, K. S. Magnetic properties of octa- and heptadeca-nuclear heterometallic Co^{II}–Ln^{III} complexes derived from the ligand 6-chloro-2-hydroxypyridine. *Polyhedron* **2013**, *66*, 48–55. (n) Zheng, Y.-Z.; Evangelisti, M.; Tuna, F.; Winpenny, R. E. P. Co–Ln Mixed-Metal Phosphonate Grids and Cages as Molecular Magnetic Refrigerants. *J. Am. Chem. Soc.* **2012**, *134*, 1057–1065. (o) Zheng, Y.-Z.; Evangelisti, M.; Winpenny, R. E. P. Co–Gd phosphonate complexes as magnetic refrigerants. *Chem. Sci.* **2011**, *2*, 99–102. (p) Costes, J.-P.; Dahan, F.; García-Tojal, J. Dinuclear Co^{II}/Gd^{III} and Co^{III}/Gd^{III} Complexes Derived from Hexadentate Schiff Bases: Synthesis, Structure, and Magnetic Properties. *Chem. - Eur. J.* **2002**, *8*, 5430–5434. (q) Zou, L.-F.; Zhao, L.; Guo, Y.-N.; Yu, G.-M.; Guo, Y.; Tang, J.; Li, Y.-H. A dodecanuclear heterometallic dysprosium–cobalt wheel exhibiting single-molecule magnet behavior. *Chem. Commun.* **2011**, *47*, 8659–8661. (r) Abtab, S. M. T.; Majee, M. C.; Maity, M.; Titis, J.; Boca, R.; Chaudhury, M. Tetranuclear Hetero-Metal [Co^{II}₂Ln^{III}₂] (Ln = Gd, Tb, Dy, Ho, La) Complexes Involving Carboxylato Bridges in a Rare μ₄–η²:η² Mode: Synthesis, Crystal Structures, and Magnetic Properties. *Inorg. Chem.* **2014**, *53*, 1295–1306. (s) Liu, Y.; Chen, Z.; ren, Z.; Zhao, X.-Q.; Cheng, P.; Zhao, B. Two-Dimensional 3d–4f Networks Containing Planar Co₄Ln₂ Clusters with Single-Molecule-Magnet

Behaviors. *Inorg. Chem.* **2012**, *51*, 7433–7435. (s) Zhao, F.-H.; Li, H.; Che, Y.-X.; Zheng, J.-M.; Vieru, V.; Chibotaru, F.; Grandjean, F.; Long, G. J. Synthesis, Structure, and Magnetic Properties of $Dy_2Co_2L_{10}(bipy)_2$ and $Ln_2Ni_2L_{10}(bipy)_2$, $Ln = La, Gd, Tb, Dy$, and Ho: Slow Magnetic Relaxation in $Dy_2Co_2L_{10}(bipy)_2$ and $Dy_2Ni_2L_{10}(bipy)_2$. *Inorg. Chem.* **2014**, *53*, 9785–9799.

(4) (a) Cui, Y.; Chen, J.-T.; Long, D.-L.; Zheng, F.-K.; Cheng, W.-D.; Huang, J.-S. Preparation, structure and preliminary magnetic studies of tri- and tetra-nuclear cobalt–lanthanide carboxylate complexes. *J. Chem. Soc., Dalton Trans.* **1998**, 2955–2956. (b) Cui, Y.; Chen, G.; Ren, J.; Qian, Y.; Huang, J. Syntheses, Structures and Magnetic Behaviors of Di- and Trinuclear Pivalate Complexes Containing Both Cobalt(II) and Lanthanide(III) Ions. *Inorg. Chem.* **2000**, *39*, 4165–4168. (c) Shiga, T.; Okawa, H.; Kitagawa, S.; Ohba, M. Stepwise Synthesis and Magnetic Control of Trimetallic Magnets $[Co_2Ln(L)_2(H_2O)_4][Cr(CN)_6] \cdot nH_2O$ ($Ln = La, Gd$; $H_2L = 2,6$ -Di-(acetoacetyl)pyridine) with 3-D Pillared-Layer Structure. *J. Am. Chem. Soc.* **2006**, *128*, 16426–16427. (d) Yang, Y.-T.; Luo, F.; Che, Y.-x.; Zheng, J.-M. Employing An Unprecedented Ferromagnetic Molecular Building Block (MBB) of $[Co_2Ln(\mu_3-OH)(CO_2)_3(N_3)]_2$ ($Ln = Tb, Gd, Dy, Eu, Sm$) to Construct a 6-Connected α -Po Net. *Cryst. Growth Des.* **2008**, *8*, 3508–3510.

(5) (a) Furniss, B. S.; Hannaford, A. J.; Smith, P. W. G.; Tatchell, A. R. *Vogel's Text book of Practical Organic Chemistry*, 5th ed.; ELBS, Longman: London, 1989. (b) Lu, J.-W.; Huang, Y.-H.; Lo, S.-I.; Wei, H.-H. New μ -oxo-bridged tetranuclear Cu(II) complex with Schiff-base ligand: Synthesis, crystal structure and magnetic properties. *Inorg. Chem. Commun.* **2007**, *10*, 1210–1213.

(6) (a) SMART & SAINT Software Reference Manuals, Version 6.45; Bruker Analytical X-ray Systems, Inc.: Madison, WI, 2003. (b) Sheldrick, G. M. SADABS, a software for empirical absorption correction, Ver. 2.05; University of Göttingen: Göttingen, Germany, 2002. (c) SHELXTL Reference Manual, Ver. 6.1; Bruker Analytical Xray Systems, Inc.: Madison, WI, 2000. (d) Sheldrick, G. M. SHELXTL, Ver. 6.12; Bruker AXS, Inc.: Madison, WI, 2001. (e) Sheldrick, G. M. A short history of SHELX. *Acta Crystallogr., Sect. A: Found. Crystallogr.* **2008**, *64*, 112–122.

(7) Bradenburg, K. *Diamond*, ver. 3.0; Crystal Impact GbR: Bonn, Germany, 2005.

(8) (a) Karmakar, S.; Khanra, S. Polynuclear coordination compounds: a magnetostructural study of ferromagnetically coupled Ni_4O_4 cubane core motif. *CrystEngComm* **2014**, *16*, 2371–2383. (b) Ahmed, N.; Das, C.; Vaidya, S.; Srivastava, A. K.; Langley, S. K.; Murray, K. S.; Shanmugam, M. Probing the magnetic and magneto-thermal properties of $M(II)$ – $Ln(III)$ complexes (where $M(II) = Ni$ or Zn ; $Ln(III) = La$ or Pr or Gd). *Dalton Trans.* **2014**, *43*, 17375–17384. (c) Ahmed, N.; Das, C.; Vaidya, S.; Srivastava, A. K.; Langley, S. K.; Murray, K. S.; Shanmugam, M. Nickel(II)–Lanthanide(III) Magnetic Exchange Coupling Influencing Single-Molecule Magnetic Features in $\{Ni_2Ln_2\}$ Complexes. *Chem. - Eur. J.* **2014**, *20*, 14235–14239.

(9) Andruh, M. The exceptionally rich coordination chemistry generated by Schiff-base ligands derived from *o*-vanillin. *Dalton Trans.* **2015**, *44*, 16633–16653.

(10) (a) Ruiz-Martínez, A.; Casanova, D.; Alvarez, S. Polyhedral Structures with an Odd Number of Vertices: Nine-Coordinate Metal Compounds. *Chem. - Eur. J.* **2008**, *14*, 1291–1303. (b) Ruiz-Martínez, A.; Casanova, D.; Alvarez, S. Polyhedral structures with an odd number of vertices: nine-atom clusters and supramolecular architectures. *Dalton Trans.* **2008**, 2583–2591. (c) Alvarez, S.; Alemany, P.; Casanova, D.; Cirera, J.; Llunell, M.; Avnir, D. Shape maps and polyhedral interconversion paths in transition metal chemistry. *Coord. Chem. Rev.* **2005**, *249*, 1693–1708.

(11) Stiefel, E. I.; Brown, G. F. Detailed nature of the six-coordinate polyhedra in tris(bidentate ligand) complexes. *Inorg. Chem.* **1972**, *11*, 434–436.

(12) Stamatatos, T. C.; Diamantopoulou, E.; Tasiopoulos, A.; Psycharis, V.; Vicente, R.; Raptopoulou, C. P.; Nastopoulos, V.; Escuer, A.; Perlepes, S. P. Enneanuclear Ni(II) complexes from the use of the flexible ligand 2-pyridinealdoxime: The nature of the inorganic

anion does not affect the chemical and structural identity of the cationic cluster. *Inorg. Chim. Acta* **2006**, *359*, 4149–4157.

(13) Nishio, M.; Hirota, M.; Umezawa, Y. *The CH/ π Interaction: Evidence, Nature, and Consequences*; Wiley–VCH: New York, 1998.

(14) (a) Klinke, F. J.; Das, A.; Demeshko, S.; Dechert, S.; Meyer, F. Inducing Single Molecule Magnetic Behavior in a $[Co_4O_4]$ Cubane via a Pronounced Solvatomagnetic Effect. *Inorg. Chem.* **2014**, *53*, 2976–2982. (b) Murrie, M.; Teat, S. J.; Stoeckli-Evans, H.; Güdel, H. U. Synthesis and Characterization of a Cobalt(II) Single-Molecule Magnet. *Angew. Chem., Int. Ed.* **2003**, *42*, 4653–4656. (c) Moubaraki, B.; Murray, K. S.; Hudson, T. A.; Robson, R. Tetranuclear and Octanuclear Cobalt(II) Citrate Cluster Single Molecule Magnets. *Eur. J. Inorg. Chem.* **2008**, *2008*, 4525–4529. (d) Galloway, K. W.; Whyte, A. M.; Wernsdorfer, W.; Sanchez-Benitez, J.; Kamenev, K. V.; Parkin, A.; Peacock, R. D.; Murrie, M. Cobalt(II) Citrate Cubane Single-Molecule Magnet. *Inorg. Chem.* **2008**, *47*, 7438–7442. (e) Guedes, G. P.; Soriano, S.; Comerlato, N. M.; Speziali, N. L.; Lahti, P. M.; Novak, M. A.; Vaz, M. G. F. Two Cobalt(II) Cubane Compounds: The Key Role of Small Ligand Changes on the Crystal Packing and Magnetic Properties. *Eur. J. Inorg. Chem.* **2012**, *2012*, 5642–5648. (f) Scheurer, A.; Ako, A. M.; Saalfrank, R. W.; Heinemann, F. W.; Hampel, F.; Petukhov, K.; Gieb, K.; Stocker, M.; Müller, P. Synthesis, Magnetic Properties, and STM Spectroscopy of Cobalt(II) Cubanes $[Co^II_4(Cl)_4(HL)_4]$. *Chem. - Eur. J.* **2010**, *16*, 4784–4792. (g) Zhang, S.-H.; Zhang, Y. D.; Zou, H. H.; Guo, J. J.; Li, H. P.; Song, Y.; Liang, H. A family of cubane cobalt and nickel clusters: Syntheses, structures and magnetic properties. *Inorg. Chim. Acta* **2013**, *396*, 119–125.

(15) (a) Meally, S. T.; McDonald, C.; Kealy, P.; Taylor, S. M.; Brechin, E. K.; Jones, L. F. Investigating the solid state hosting abilities of homo- and hetero-valent $[Co_7]$ metallocalix[6]arenes. *Dalton Trans.* **2012**, *41*, 5610–5616. (b) Zhang, S.-H.; Song, Y.; Liang, H.; Zeng, M.-H. Microwave-assisted synthesis, crystal structure and properties of a disc-like heptanuclear Co(II) cluster and a heterometallic cubanic Co(II) cluster. *CrystEngComm* **2009**, *11*, 865–872. (c) Wei, L.-Q.; Li, B.-W.; Hu, S.; Zeng, M.-H. Controlled assemblies of hepta- and trideca- Co^II clusters by a rational derivation of salicylaldehyde Schiff bases: microwave-assisted synthesis, crystal structures, ESI-MS solution analysis and magnetic properties. *CrystEngComm* **2011**, *13*, 510–516.

(16) (a) Bartolomé, J.; Filoti, G.; Kuncser, V.; Schinteie, G.; Mereacre, V.; Anson, C. E.; Powell, A. K.; Prodius, D.; Turta, C. Magnetostructural correlations in the tetranuclear series of $\{Fe_3LnO_2\}$ butterfly core clusters: Magnetic and Mössbauer spectroscopic study. *Phys. Rev. B: Condens. Matter Mater. Phys.* **2009**, *80*, 14430. (b) Ishikawa, R.; Miyamoto, R.; Nojiri, H.; Breedlove, B. K.; Yamashita, M. Slow Relaxation of the Magnetization of an Mn^{III} Single Ion. *Inorg. Chem.* **2013**, *52*, 8300–8302.